SISSA

PAPER

Consequences for predator–prey dynamics caused by the presence of obstacles

View the article online for updates and enhancements.

PAPER: Interdisciplinary statistical mechanics

Consequences for predator–prey dynamics caused by the presence of obstacles

J R Šćepanović[1,*], Lj Budinski-Petković[2], Z M Jakšić[1], A Belić[1] and S B Vrhovac[1]

[1] Institute of Physics Belgrade, University of Belgrade, Pregrevica 118, Zemun, 11080 Belgrade, Serbia
[2] Faculty of Engineering, Trg D. Obradovića 6, Novi Sad 21000, Serbia
E-mail: julija@ipb.ac.rs

Abstract. In order to understand how a heterogeneous habitat affects the population dynamics of the predator–prey system, a spatially explicit lattice model consisting of predators, prey and obstacles is constructed. The model includes smart pursuit (predators to prey) and evasion (prey from predators). Both species can affect their movement by visual perception within their finite sighting range. Non-conservative processes that change the number of individuals within the population, such as breeding and physiological dying, are implemented in the model. Obstacles are represented by non-overlapping lattice shapes that are randomly placed on the lattice. In the absence of obstacles, numerical simulations reveal regular, coherent oscillations with a nearly constant predator–prey phase difference. Numerical simulations have shown that changing the probabilities for non-conservative processes can increase or decrease the period of coherent oscillations in species abundances and change the relative lag between coherent components. After introducing obstacles into the model, we observe random transitions between coherent and non-coherent oscillating regimes. In the non-coherent regime, predator and prey abundances continue to oscillate, but without a well-defined phase relationship. Our model suggests that stochasticity introduced by density fluctuations of obstacles is responsible for the reversible shift from coherent to non-coherent oscillations.

*Author to whom any correspondence should be addressed.

Contents

1. Introduction

In predator–prey modeling, a system is modeled as a collection of autonomous decision-making entities called agents. Basically, two types of agents are present in the system: chasers (predators) and escapees (prey). A predator–prey model consists of a system of agents and the relationships between them. Each agent individually assesses its situation and makes decisions on the basis of a set of rules. Predator–prey models can exhibit complex behavior patterns and provide valuable information about the dynamics of real-world systems. For example, simple predator–prey models may exhibit limit cycles during which the populations of both species have periodic oscillations in time with a 1/4-period lag between predator and prey [1–4]. These oscillations in species abundances have been successfully observed in nature [5–8]. Furthermore, the predator–prey systems have been studied in various contexts, such as robotics, game theory and ecology [9–15].

Habitat heterogeneity has long been recognized as a major factor in ecological dynamics. Animal habitats include natural physical obstacles, such as lakes, rivers or high mountains and areas of avoidance due to increased predation risk such as open

areas without refuge. In addition, habitats are often intersected by long human-made structures, such as roads, railways, power lines and pipe lines [16, 17]. These spatial heterogeneities can affect predator–prey interactions in two qualitatively different ways, by providing refuge for the prey or obstacles that interfere with the movements of both prey and predators. Predation is a consequence of predators and prey overlapping (i.e. encounters) in time and space. Animals regulate the encounter process by deciding which parts of resource to use, how long to use these parts, and how to travel among them. However, anthropogenic landscape changes can alter the animals' ability to access resources and avoid predation, with consequences for predator–prey dynamics [18–20]. In this paper, we aim to explore how habitat spatial obstacles may affect the predator–prey dynamics. Special attention is paid to the changes in the oscillatory properties of species abundances caused by the presence of obstacles.

In the following, we sketch the main features of our numerical model, along the lines of [21, 22]. Our model is an agent-based approach to simulate numerically collective chasing and escaping in a discrete space with periodic boundary conditions. Our approach is similar to the model of hunting in groups proposed by Kamimura and Ohira [23–25]. The problem of group chase and escape in various situations and extensions has been studied by computer simulations and by theoretical analysis. Examples include the model with conversion of caught escapees into chasers [26], the group chase and escape by three groups [27], the models with fast chasers [28], the group chase and escape model with the chaser's interaction [29], the off-lattice model [30], the three aggregation strategies for the prey [31], etc. Predators and prey are initially placed randomly on the sites of the square lattice as pointlike particles. Distances in the present study are measured by the L^1 ('Manhattan') metric. For example, the site (x, y) is at distance $|x| + |y|$ from the origin, with the lattice spacing equal to unity. Both species perform independent nearest-neighbor walks on a lattice following simple dynamical rules, increasing or decreasing the distance from the nearest particle of the opposite group. Each species has its specific sighting range σ in which it can see the other species. Predators (prey) can sense the position of the prey (predator) at a predefined distance σ and they try to move to one of the nearest neighboring sites in order to decrease (increase) the distance from the nearest prey (predator). Therefore, the sighting range σ describes their skills at chasing or escaping. Prey is caught upon the first encounter with a predator. Analysis of the capture dynamics in the present study is limited to species with the same sighting ranges, i.e. $\sigma = 2$ [21, 22]. If the value of σ is equal to zero, the movement is equivalent to that of random walkers [23, 26, 32, 33]. It has been confirmed that the idea of animals using blind search strategies does not seem to be usable since it neglects the role of animal intelligence and experience in guiding them [34]. Consequently, we have not considered species with zero sighting range.

Non-conservative processes that change the number of individuals (size of the population), such as breeding and physiological dying, are also implemented in the model [22, 32, 35–38]. The model contains five parameters that control the non-conservative processes. The birth and two death rates of predators and two parameters characterizing the birth and death of prey. In the presence of non-conservative processes, the dominant type of dynamics can be characterized by regular, coherent oscillations in time with a nearly constant predator–prey phase difference [1–4]. These oscillations in

species abundances have been successfully observed in real-world systems or laboratory studies with fast-reproducing organisms [5–8, 39, 40].

Furthermore, an element of stochasticity of the environment, such as obstacles present in any natural system, is incorporated into the model. Lattice-based models allow easy handling of obstacles of various shapes and sizes. We study the case when the lattice is initially covered with obstacles at various concentrations. Depositing objects (obstacles) of various shapes are formed by a small number of lattice steps on the square lattice. The spatial distribution of the obstacles on the lattice is created using the random sequential adsorption (RSA) method [41, 42].

In addition to the empirical data, long-running experiments with fast-reproducing organisms also support the sustained nature of predator–prey cycles [6, 39, 40, 43–45]. Since these experiments can be carried out under controlled conditions, they are suitable for finding the most important parameters that influence the species dynamics and coexistence. Recently, the potential for long-term persistence of predator–prey cycles has been experimentally studied with a planktonic predator–prey system [45]. Experiments were conducted with parthenogenetic rotifers as predators and unicellular algae as prey under constant environmental conditions. Although the experiments were not perturbed by external influences, transitions between two different dynamic regimes were identified. Periods in which the predator densities follow the prey densities with a phase lag of about $\pi/2$ (coherent oscillations) were intersected by non-coherent oscillation regimes in which a well-defined phase relationship between the measured signals is lost. We show that the stochasticity introduced by the presence of obstacles can be responsible for the reversible shift from coherent to non-coherent oscillations.

We organized the paper as follows. Section 2 describes the details of the model and simulations. In section 3, results of numerical simulations are presented and discussed. Section 4 contains some additional comments and final remarks. Some technical details of the calculations are given in the appendices.

2. Definition of the model and the simulation method

The environment where two interacting species coexist is represented by a two-dimensional square lattice of linear size $L = 256$ with periodic boundary conditions. The lattice is initially occupied by obstacles of various shapes and sizes. Their spatial distribution at density ρ_0 is generated using the RSA method [41, 42]. This density ρ_0 is defined as the fraction of sites of the lattice that are occupied by the obstacles. Linear obstacles are k-mers of length $\ell = 0, 1, \ldots, 8$, shown in table 1 as objects (A_1)–(A_9).

To initialize the numerical simulations, $N_1^{(0)}$ predators and $N_2^{(0)}$ prey are randomly distributed as monomers in the lattice up to the chosen densities $\rho_1^{(0)} = N_1^{(0)}/L^2$ and $\rho_2^{(0)} = N_2^{(0)}/L^2$. Again, the initial spatial distribution of species on the lattice is generated using the RSA method [41, 42]. Accordingly, each site can be either empty or occupied by one particle: a chaser (predator), an escapee (prey) or a particle that belongs to an obstacle.

Table 1. Jamming coverages $\rho_{\mathrm{J}}^{(x)}$ for various k-mers (x) of length $\ell^{(x)}$ on a square lattice [46].

(x)	k-mer	$\ell^{(x)}$	$\rho_{\mathrm{J}}^{(x)}$
(A_1)	·	0	1.0
(A_2)	⊶	1	0.9067
(A_3)	⊶	2	0.8465
(A_4)	⊶	3	0.8102
(A_5)	⊶	4	0.7867
(A_6)	⊶	5	0.7699
(A_7)	⊶	6	0.7578
(A_8)	⊶	7	0.7479
(A_9)	⊶	8	0.7405

2.1. Movement of predators and prey

The movement of individuals with escape and pursuit behavior within the lattice is modeled as a discrete-time process. At this stage, apart from the hard-core interaction between the species and between the species and the obstacles, there are simple rules governing the dynamic processes at an individual level. At each Monte Carlo step, a lattice site is selected at random. If the chosen site is unoccupied, the positions of predators and prey remain unchanged, and a new site is randomly selected. If a predator or prey occupies the chosen site, each species follows the hopping rules described below. After each Monte Carlo step, the time t is updated, $t \rightarrow t + 1/L^2$, and the process continues by randomly choosing a new lattice site. The present model includes species with the same sighting range, $\sigma = 2$. Accordingly, the decision for every step, both of the predator and prey depends on the individuals and obstacles that are found at the places of the first and second neighbors.

Suppose that the predator is placed in a randomly selected site of the lattice. If the first neighbors of the selected site are entirely occupied by obstacles and predators, the chosen predator stays at its original position. Then, the time t is updated, and the process continues by selecting a new lattice site at random. Suppose that some of the first neighbors of the selected site are occupied by prey. Then, we randomly select a prey among them, remove it from the lattice, and move the chosen predator to this empty place. However, if the first neighbors of the selected predator are not occupied by prey, the predator executes a jump as long as there is at least one empty nearest neighbor site. In this case, the predator moves to the vacant adjacent site surrounded by the highest number of prey, $n_2^{(\mathrm{max})}$, as its first neighbors. If two or more empty nearest neighbor sites correspond to the same highest number of prey, $n_2^{(\mathrm{max})}$, one of them is selected at random.

Suppose that the prey is placed in a randomly selected lattice site. If there are no empty nearest neighbors of the selected site, the chosen prey does not change its position, and the time increases by $1/L^2$. The process continues by choosing a new lattice site at random. If the selected site has empty adjacent sites, the chosen prey jumps to

the vacant nearest neighbor site surrounded by the lowest number of predators, $n_1^{(\min)}$, as its first neighbors. If two or more empty nearest neighbor sites correspond to the same lowest number of predators, $n_1^{(\min)}$, one of them is selected at random. It must be emphasized that a prey moves to the selected site only if $n_1^{(\min)}$ is less than or equal to the number of predators surrounding it in its original position.

2.2. Non-conservative processes

We introduce into the model the following non-conservative processes and an additional set of rules that define the population dynamics.

Rules intended for predators:

1. Predators that have eaten prey during the displacement can leave offspring at the previously occupied site, with probability P_{1b}^{fed} (birth probability of predators). To breed, the predator must be strong enough, i.e. it must have food available in the immediate vicinity.
2. Predators that have not eaten prey during the displacement can die with probability P_{1d}^{unfed}. It is assumed that the lack of food reduces the number of predators in the habitat.
3. Predators can suddenly die with probability P_{1d} (death probability of predators).

Rules intended for prey:

1. After displacement, prey can leave offspring filling an empty previously occupied site with probability P_{2b} (birth probability of prey).
2. Prey has a probability P_{2d} of dying (death probability of prey).

Species mortality probabilities P_{1d} and P_{2d} quantitatively describe dying that could be related to various factors and events in the ecosystem, such as the age of individuals or diseases. Here, we list the probability values that characterize non-conservative processes as sequences of numbers with the following structure: $\mathcal{S} = \{P_{1b}^{\mathrm{fed}}, P_{1d}^{\mathrm{unfed}}, P_{1d}; P_{2b}, P_{2d}\}$.

2.3. Algorithm

Based on the above definitions and rules, we formulate the algorithm as follows. If a randomly selected site of the lattice is not empty, the predator (prey) can die with probability P_{1d} (P_{2d}). If the predator (prey) dies, it is removed from the lattice, and a new site is selected. Otherwise, we apply the rules for the pursuit–evasion movement for individuals explained above (section 2.1). If the randomly selected predator survives, we check whether it ate the prey during the displacement. If so, the predator leaves an offspring at the previously occupied site, with probability P_{1b}^{fed}. However, if the predator did not eat the prey during the displacement, it dies with probability P_{1d}^{unfed}. Similarly, if the randomly selected prey survives, we check whether it moved into a new position. If so, the prey leaves an offspring at the previously occupied site, with probability P_{2b}.

3. Results and discussion

In the first part of this section, the group spatial chase and escape phenomena are analyzed in the environment without heterogeneities. Then, population dynamics are studied in an environment that contains spatial obstacles.

3.1. Dynamics of the system without obstacles

In figures 1 and 2, we present numerical results regarding the time evolution of the normalized number of predators, $\tilde{N}_1(t) = N_1(t)/N_1^{(0)}$, and prey, $\tilde{N}_2(t) = N_2(t)/N_2^{(0)}$, for the two representative sets of probabilities that characterize the non-conservative processes: $\mathcal{S}_1 = \{0.09, 0.05, 0.01; 0.15, 0.01\}$ and $\mathcal{S}_2 = \{0.25, 0.10, 0.01; 0.20, 0.01\}$. For both cases, the initial numbers of species were chosen as $N_1^{(0)} = 2880$ and $N_2^{(0)} = 3200$, corresponding to the initial densities $\rho_1^{(0)} = N_1^{(0)}/L^2 = 0.0439$ and $\rho_2^{(0)} = N_2^{(0)}/L^2 = 0.0488$, with the ratio $\rho_1^{(0)}/\rho_2^{(0)} = N_1^{(0)}/N_2^{(0)} = 0.90$. It is important to note that the time evolution of the normalized number of species $\tilde{N}_1(t)$ and $\tilde{N}_2(t)$ does not depend on the lattice size L if the initial densities $\rho_1^{(0)}$ and $\rho_2^{(0)}$ of species do not change with L [22]. However, for a lattice of fixed size L, the time evolution of $\tilde{N}_1(t)$ and $\tilde{N}_2(t)$ depends on the initial number (density) of predators $N_1^{(0)}$ and prey $N_2^{(0)}$.

Let us compare the results for two different sets of probabilities $\mathcal{S}_1$ and $\mathcal{S}_2$, shown in figures 1(a) and 2(a). We show that the time dependencies of the normalized number of species $\tilde{N}_1(t)$ and $\tilde{N}_2(t)$ are qualitatively similar. In the initial stage, the number of predators and prey oscillates periodically with large amplitudes, rapidly decreasing in time. After a short transient period, the system arrives at a quasi-steady state. This state corresponds to coexisting populations of predators and prey when their densities oscillate around some average values, which do not change over time.

More details about the temporal behavior of the number of predators and prey for the quasi-steady state stage of evolution, in the time range between $t_1 = 4000$ u.t. and $t_2 = 5000$ u.t. are shown in figures 1(b) and 2(b). Our model provides the usual prediction that in predator–prey cycles, the peaks in prey abundance precede the peaks in predator abundance [4]. When predators are sparse, prey increase and are in abundance. As the number of prey increases, predators also increase and are in abundance. When the predators reach sufficiently high densities, the prey population is driven down to low densities. With a lack of prey, the predator population reduces, and the cycle repeats.

It is interesting to compare the oscillatory behavior of the number of predators $\tilde{N}_1(t)$ and prey $\tilde{N}_2(t)$ in the quasi-steady state regime obtained for two different sets of probabilities, $\mathcal{S}_1$ and $\mathcal{S}_2$, that characterize the non-conservative processes (see figures 1(b) and 2(b)). It is obvious that the change of probabilities from $\mathcal{S}_1$ to $\mathcal{S}_2$ leads to an increase in the frequency of oscillations of the number of predators and prey. We investigate the species fluctuations in further detail using a wavelet analysis, which reveals statistically significant associations between the dynamics of the predator and prey densities [47, 48]. Details of the power analysis and the phase analysis (in particular, cross-wavelet analysis and wavelet coherence (WCO)) are given in the appendix.
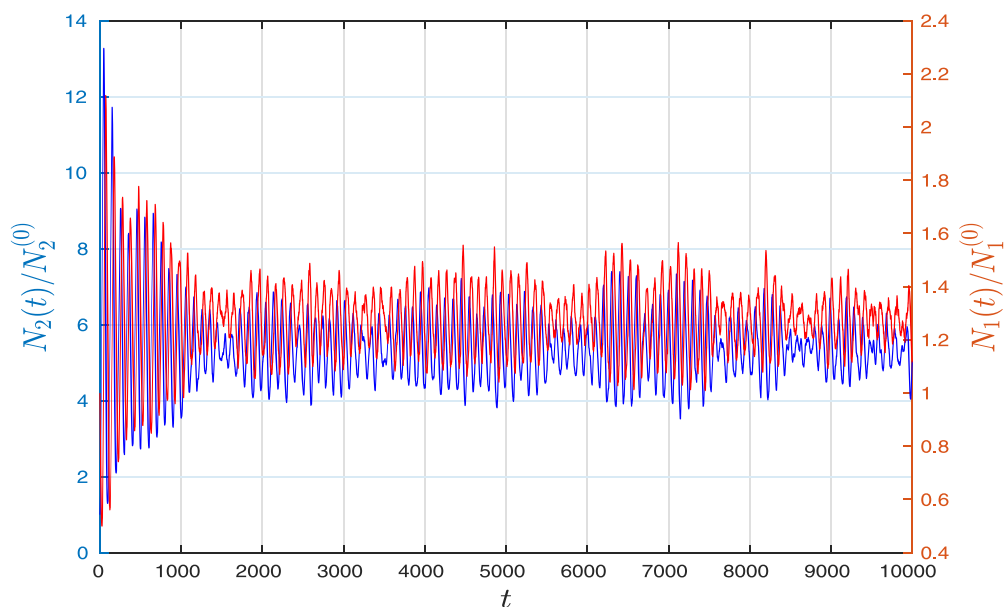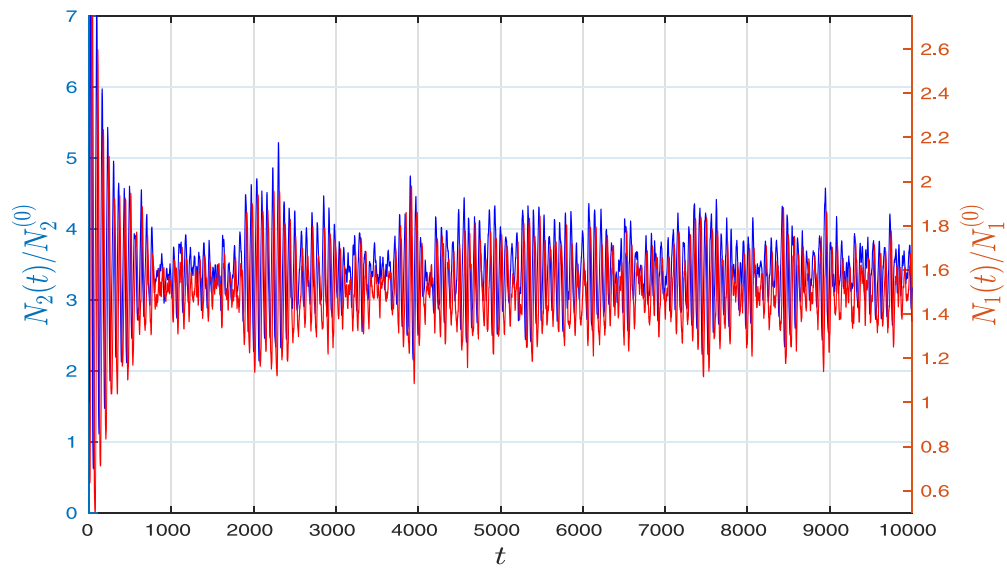
(a)
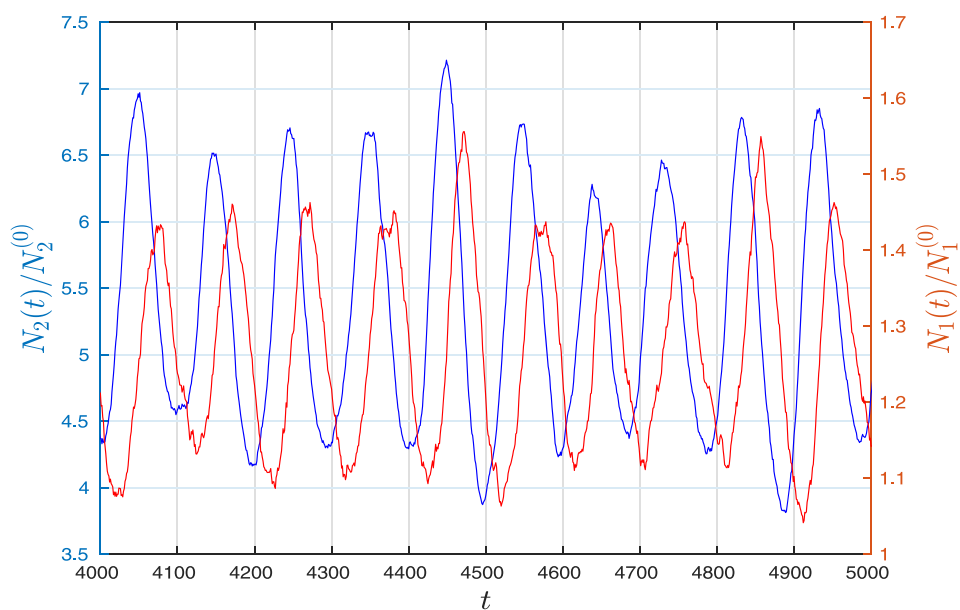
(b)

Figure 1. (a) Time dependencies of the number of the normalized number of predators $\tilde{N}_1 = N_1(t)/N_1^{(0)}$ (red lines) and prey $\tilde{N}_2 = N_2(t)/N_2^{(0)}$ (blue lines) on the lattice of size $L = 256$. Initial numbers of species are chosen as $N_1^{(0)} = 2880$ and $N_2^{(0)} = 3200$. Probabilities that characterize the non-conservative processes are $\mathcal{S}_1 = \{0.09, 0.05, 0.01, 0.15, 0.01\}$. (b) Shown here are the temporal dependencies of the $\tilde{N}_1$ and $\tilde{N}_2$ in the oscillatory region of the quasi-steady state, between $t_1 = 4000$ u.t. and $t_2 = 5000$ u.t., taken from the panel (a).
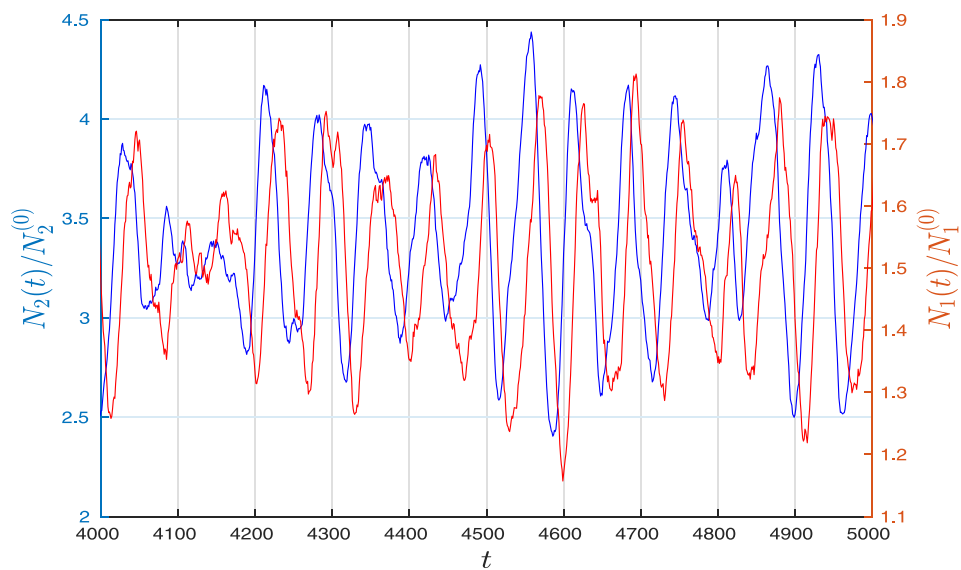
(a)

(b)

Figure 2. (a) Time dependencies of the number of the normalized number of predators $\tilde{N}_1 = N_1(t)/N_1^{(0)}$ (red lines) and prey $\tilde{N}_2 = N_2(t)/N_2^{(0)}$ (blue lines) on the lattice of size $L = 256$. Initial numbers of species are chosen as $N_1^{(0)} = 2880$ and $N_2^{(0)} = 3200$. Probabilities that characterize the non-conservative processes are $\mathcal{S}_2 = \{0.25, 0.10, 0.01, 0.20, 0.01\}$. (b) Shown here are the temporal dependencies of the $\tilde{N}_1$ and $\tilde{N}_2$ in the oscillatory region of the quasi-steady state, between $t_1 = 4000$ u.t. and $t_2 = 5000$ u.t., taken from the panel (a).
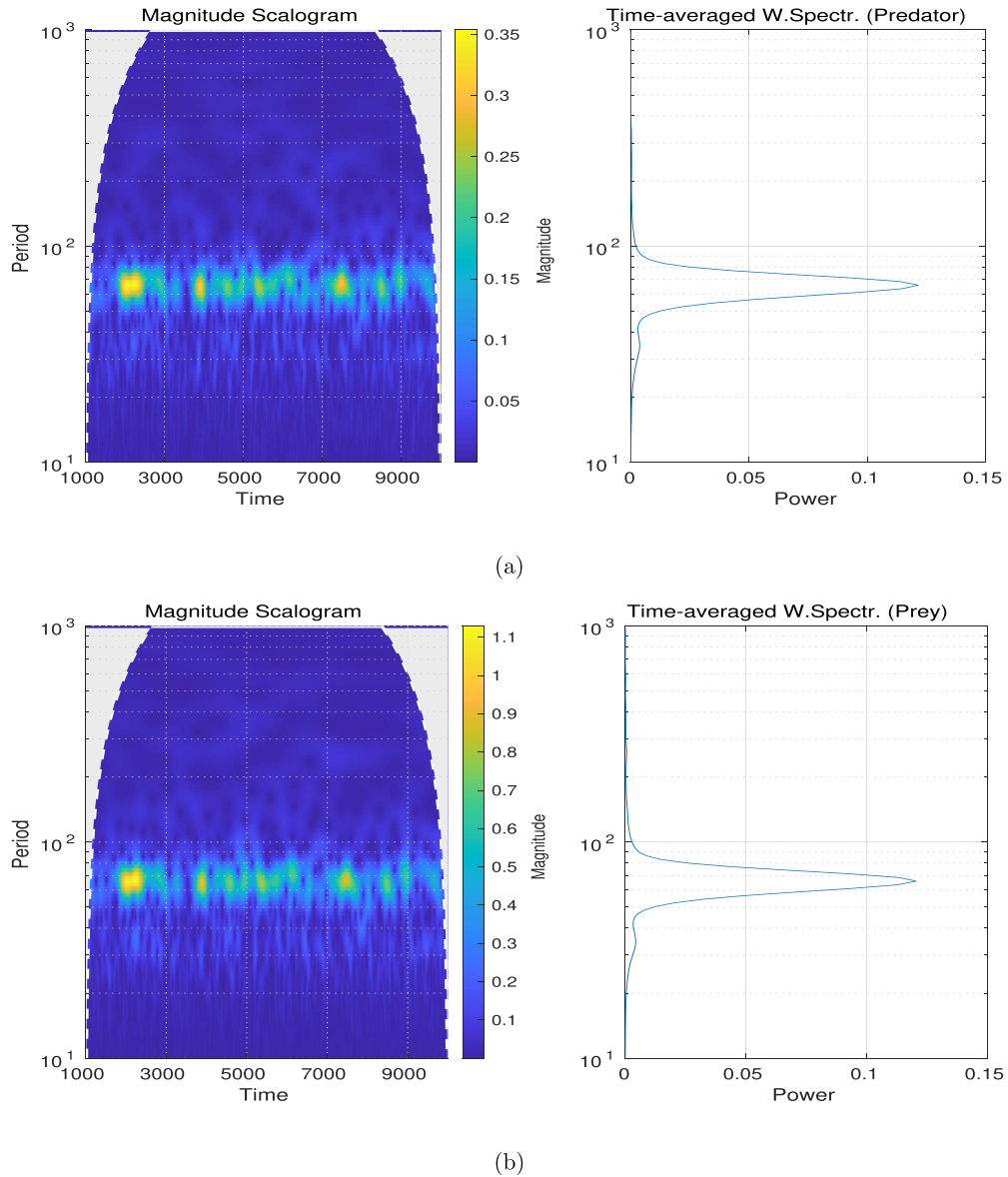
(a)

(b)
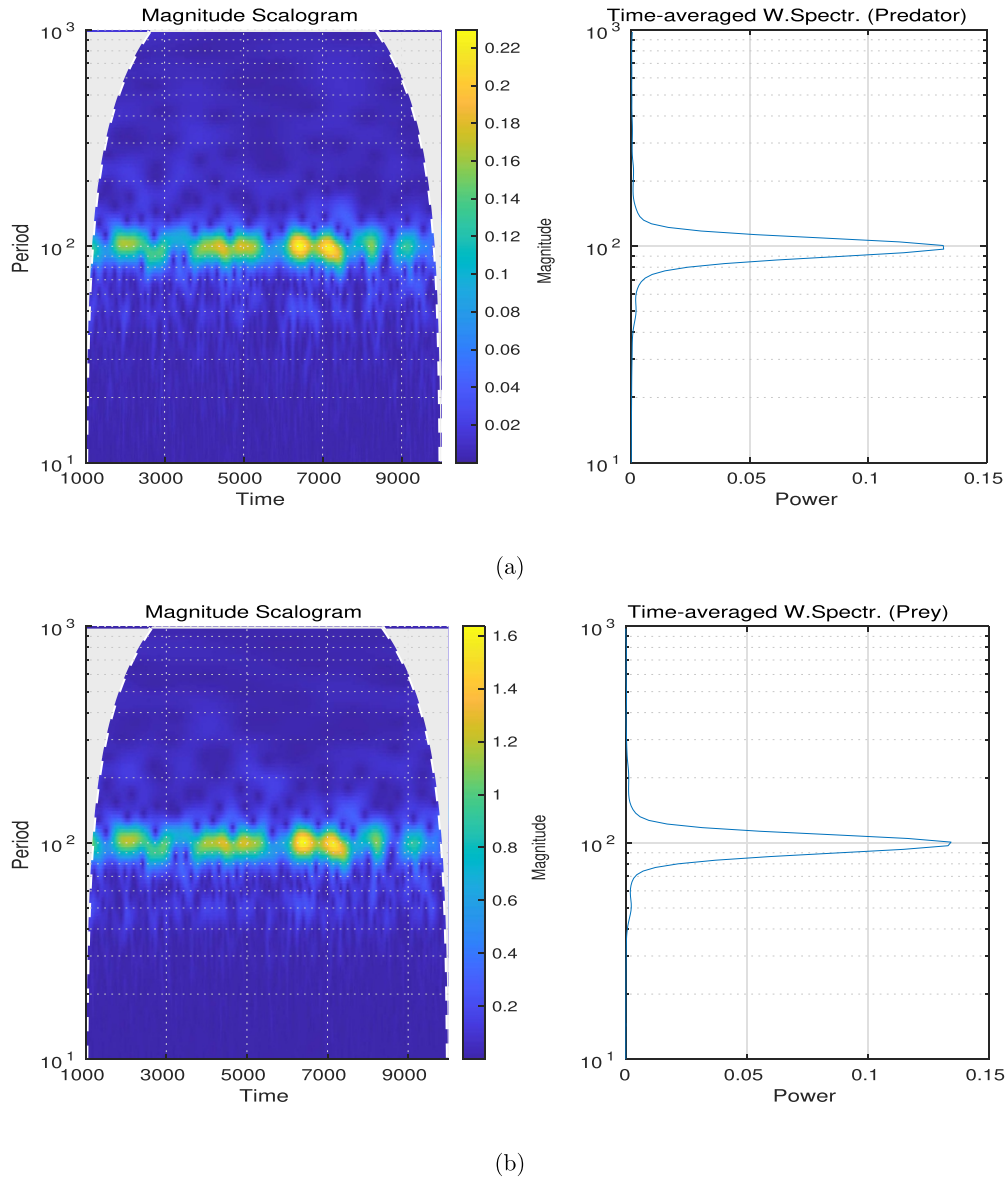
Figure 3. Scalograms and time-averaged wavelet power spectra of the predator and prey time series, $\tilde{N}_1(t)$ (a) and $\tilde{N}_2(t)$ (b) respectively, corresponding to the quasi-steady state regime of evolution ($t > 1000$ u.t.). Probabilities that characterize the non-conservative processes are $\mathcal{S}_1 = \{0.09, 0.05, 0.01, 0.15, 0.01\}$.

In figure 3, we show the scalograms and the time-averaged power spectra of the signals $\tilde{N}_1(t)$ and $\tilde{N}_2(t)$ obtained for the same conditions as in figure 1. The scalogram is the absolute value of the continuous wavelet transform (CWT) plotted as a function of time and frequency (i.e. period). Time-averaged power spectra are obtained by time-averaging the magnitude-squared scalogram over all times. The period is plotted on a logarithmic scale. The cone of influence showing where edge effects become significant is also plotted. Gray regions outside the dashed white line delineate regions where edge

(a)

(b)

Figure 4. Scalograms and time-averaged wavelet power spectrum of the predator and prey time series, $\tilde{N}_1(t)$ (a) and $\tilde{N}_2(t)$ (b) respectively, corresponding to the quasi-steady state regime of evolution ($t > 1000$ u.t.). Probabilities that characterize the non-conservative processes are $\mathcal{S}_2 = \{0.25, 0.10, 0.01, 0.20, 0.01\}$.

effects are significant. Here, we normalize the power of the time-averaged wavelet spectrum as a probability density function. CWT gives a time-frequency representation that accurately captures the instantaneous frequencies of the signals $\tilde{N}_1(t)$ and $\tilde{N}_2(t)$. Both for predators and prey, the CWT shows nearly steady-state oscillations with the same period of about $T_1 = 97$ u.t.. This value corresponds to the position of the maximum in the time-averaged wavelet spectra (see the right-hand-side panels in figure 3).

The scalograms and the time-averaged power spectra of the signals $\tilde{N}_1(t)$ and $\tilde{N}_2(t)$ from figure 2, which correspond to the set of probabilities $\mathcal{S}_2$, are presented in figure 4.

Figures 3 and 4 enable a quantitative comparison of the oscillatory behavior of the number of predators and prey for the two sets of probability values $\mathcal{S}_1$ and $\mathcal{S}_2$ that characterize the non-conservative processes. For the set $\mathcal{S}_2$, numerical simulations revealed sustained oscillations with a shorter period length of $T_2 = 64$ u.t.. In the second set of parameters $\mathcal{S}_2$, the probabilities P_{1b}^{fed}, P_{1d}^{unfed} and P_{2b} for the non-conservative processes related to predator feeding and prey reproduction are significantly enhanced. The predator–prey cycles are based on a feeding relationship between two species. We consider the case where the coupling between the predator and prey systems is much stronger in the case of parameters from set $\mathcal{S}_2$. Consequently, the period of oscillations of species in the quasi-stationary regime corresponding to the set of parameters $\mathcal{S}_2$ is smaller than in the case of the set of parameters $\mathcal{S}_1$.

The previously mentioned reasons for the change of the period of oscillations in species abundances are confirmed by the results of additional numerical simulations. For instance, numerical simulations have shown that increasing the probability P_{2b} is a sufficient condition for decreasing the period of oscillations. Increasing the probability P_{2b} tends to hasten the growth of the prey population. The increased food availability and better nutrition hasten the growth of the number of predators. Faster growth of the predator population shortens the time required for the number of prey to reach the maximum value. Then, the increased number of predators leads to an accelerated decrease in the prey number. The resulting lack of food shortens the time needed for the number of predators to reach a maximum value and begin to decline.

3.1.1. Coherence of the fluctuations Often the two signals are related in some way, e.g. one signal may determine behavior in another. The signals may also be correlated due to some influence intrinsic to both signals. Fourier-domain coherence is a well-established technique for measuring the linear correlation between two stationary processes as a function of frequency. Since wavelets provide local information about data in time and scale (frequency), wavelet-based coherence allows us to measure the time-varying correlation as a function of frequency. Consequently, a WCO is suitable for nonstationary processes, such as predator–prey coexistence. The WCO measures the correlations between the fluctuations of two time series (i.e. the coherence of the fluctuations). Wavelet coherency is defined as the wavelet cross-spectrum (WCS) normalized by the spectrum of each signal (see appendix).
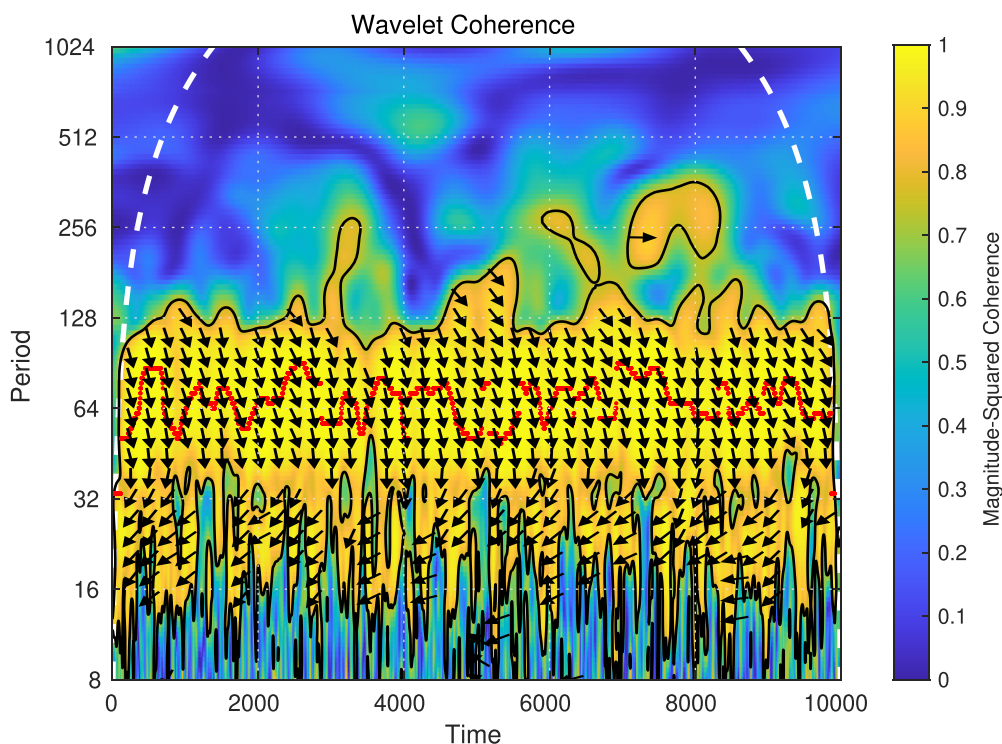
In figure 5, we show the WCO between predators and prey obtained from the numerical data shown in figure 1(a). Color coding indicates the WCO, while arrows indicate the phase angles between the fluctuations of the two time series. The black contour lines enclose significant areas (95% significance level). The red dots show the instantaneous oscillation period $\tilde{s}(t)$ of the highest WCO within these areas (coherent oscillation regimes). To clarify the diagram, only in regions of the time-frequency (period) plane where WCO exceeds 0.85, is the phase of the WCS used to indicate the relative lag between coherent components. Note that a 1/4 cycle lag between the two signals at a particular frequency is indicated by an arrow pointing vertically down. The white dashed line shows a cone of influence where edge effects become significant at different frequencies (scales). It is evident that oscillations corresponding to the set of probabilities $\mathcal{S}_1$ are persistently coherent, meaning that the ups and downs of the different species in the
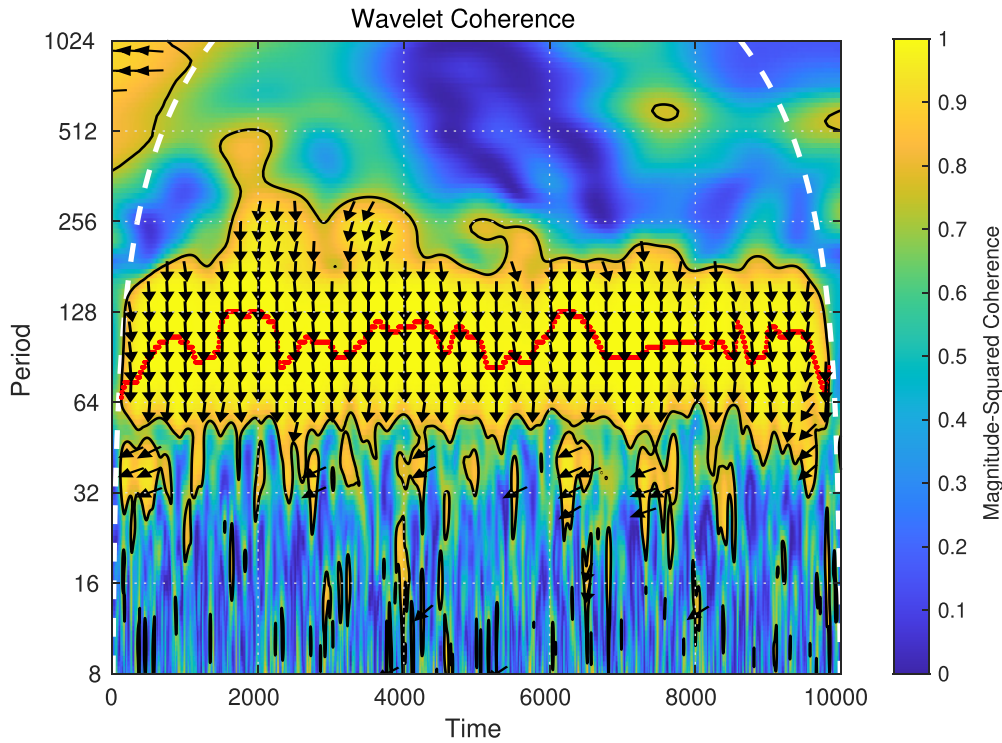
Figure 5. WCO between predators and prey, corresponding to time series $\tilde{N}_1(t)$ and $\tilde{N}_2(t)$ shown in figure 1(a). Values range from 0 (blue) to 1 (yellow). Cone of influence is indicated by the dashed white lines. Red dots indicate the instantaneous oscillation period $\tilde{s}(t)$ of the highest WCO within the prefixed period length band (64–256 u.t.). Significant areas (95% significance level) are enclosed by thin solid lines. Arrows indicate the phase angles between the fluctuations of the two species. Arrows pointing down represent a 1/4 cycle delay between the two time series. Clockwise (counterclockwise) arrow rotation corresponds to an increase (decrease) in phase lag between them. We use the phase display threshold of 0.85, which shows phase arrows only where the coherence is greater than or equal to 0.85.

predator–prey community are indeed related to each other. For the whole quasi-state regime, we observe oscillations of period of about $T_1 = 97$ u.t. both for predators and prey, with a significantly coherent, nearly constant phase relationship. These sustained cycles are also reflected in the clockwise motion in the predator–prey phase plane. More precisely, the predator densities follow the prey densities with a phase lag of about $\pi/2$ at frequencies $1/T_1$. A quarter delay (phase angle of $\pi/2$) between the fluctuations of predator and prey species is typical for many predator–prey models (e.g. [49]).

Figure 6 shows the WCO between predators and prey obtained from the time series shown in figure 2(a). The dominant type of dynamics is characterized by regular, coherent oscillations with a nearly constant predator–prey phase difference. In fact, the two species fluctuate at a significant periodicity of $T_2 = 64$ u.t. but the arrows now indicate a phase angle noticeably smaller than $\pi/2$. These phase differences are notably constant over all different numerical simulation replicates. An increase in the probability of predator breeding P_{1b}^{fed} tends to accelerate the growth of the number of predators. The

Figure 6. WCO between predators and prey, corresponding to time series $\tilde{N}_1(t)$ and $\tilde{N}_2(t)$ shown in figure 2(a). Values range from 0 (blue) to 1 (yellow). Cone of influence is indicated by the dashed white lines. Red dots indicate the instantaneous oscillation period $\tilde{s}(t)$ of the highest WCO within the prefixed period length band (32–256 u.t.). Significant areas (95% significance level) are enclosed by thin solid lines. Arrows indicate the phase angles between the fluctuations of the two species. Arrows pointing down represent a 1/4 cycle delay between the two time series. Clockwise (counterclockwise) arrow rotation corresponds to an increase (decrease) in phase lag between them. We use the phase display threshold of 0.85, which shows phase arrows only where the coherence is greater than or equal to 0.85.

faster growth of the predator population slows the growth of the number of prey. These processes shorten the time between reaching two successive maxima, i.e. the maxima for the time dependencies of predators $\tilde{N}_1(t)$ and prey $\tilde{N}_2(t)$.

3.2. Dynamics of the system with obstacles

Here, we consider in more detail the influence of the length ℓ and density ρ_0 of the linear segments that cause the obstacles on the temporal behavior of the number of predators $\tilde{N}_1(t)$ and prey $\tilde{N}_2(t)$. Simulations have been performed for linear segments (k-mers) of lengths $\ell = k - 1$, $k = 1, 2, \ldots, 9$ (see, table 1), and for a wide range of obstacle densities, $\rho_0 = 0 - 0.25$, below the corresponding percolation thresholds [50, 51]. As the density of obstacles is increased above a percolation threshold p_c^*, the initial large cluster of empty lattice space breaks into tiny non-communicating components so that connectivity between both sides of the lattice disappears. In this case, spatially separated groups

of predators and prey can be formed on the lattice during the initialization process. These artificial situations will not be considered in this paper.

We begin the analysis of habitat heterogeneity's impact on predator–prey coexistence dynamics with a quantitative description of the interaction of individuals with obstacles. In our model, there is a hard-core interaction between the individuals and the obstacles. We consider that grid nodes that form the obstacles are inaccessible to predators and prey. When the obstacle is located at the place of the first neighbor, it affects the individual's decision about where to go. Accordingly, predators and prey will never choose a direction of movement towards a neighboring node where an obstacle is located. They 'see' the obstacles and 'wisely' determine the direction of their movement , following the movement rules provided in section 2.1. It is stated that prey always move towards lower predator concentration. Predators, in the absence of prey as their immediate neighbors, move towards higher prey concentration. Although collisions of individuals with obstacles (in the sense of particle collision with a wall) do not formally exist, it is necessary to quantitatively characterize their interaction with obstacles. Therefore, we count the movements of predators and prey in which at least one first neighbor is occupied by an obstacle while selecting the direction of their motion. The number of such 'encounters' between predators (prey) and obstacles per unit of time normalized to one individual, is called the collision frequency, ν.

The temporal behavior of the collisional frequencies of predators (ν_1) and prey (ν_2) for the quasi-steady state stage of evolution ($t = 4000 - 6000$) in the presence of obstacles (4-mers) are shown in figure 7. The numerical results correspond to a set of probabilities $\mathcal{S}_1 = \{0.09, 0.05, 0.01, 0.15, 0.01\}$, and two densities of 4-mers, $\rho_0 = 0.15,\ 0.25$. At both densities of the obstacles, the collision frequency of prey ν_2 is higher than the collision frequency of predator ν_1. Indeed, when avoiding predators, prey move towards areas where the predator population is smaller. These areas often contain a higher concentration of obstacles. The movement of prey towards regions of higher concentration of obstacles increases the collision frequency of ν_2. As expected, increasing the density of obstacles ρ_0 increases the collision frequencies of both species with obstacles.

In figure 8, we show the time-averaged wavelet power spectrum (WPS) of the time-series $\tilde{N}_1(t)$ and $\tilde{N}_2(t)$ obtained for the set of probabilities $\mathcal{S}_1 = \{0.09, 0.05, 0.01, 0.15, 0.01\}$, in the presence of obstacles (9-mers) at various densities $\rho_0 = 0,\ 0.10,\ 0.15,\ 0.20,\ 0.25$. It is observed that the maximum of the global WPS shifts to higher values with the increase in the density of obstacles ρ_0. This shift indicates an increase in the mean oscillation period T of the time series $\tilde{N}_1(t)$ and $\tilde{N}_2(t)$. The period T grows from $T \approx 97$ u.t. to $T \approx 112$ u.t. when the density of obstacles ρ_0 increases from 0 to 0.25. Hence, the presence of obstacles in the habitat slightly slows down the dynamics of a group chasing and escaping between predators and prey. In addition, increasing the density of obstacles ρ_0 leads to a broadening of the peak in the global WPS. Time-averaged WPS measures the averaged variance of the time-series $\tilde{N}_1(t)$ and $\tilde{N}_2(t)$ at scale s (see appendix). Accordingly, the presence of obstacles increases the deviations of the oscillatory period T of the time-series $\tilde{N}_1(t)$ and $\tilde{N}_2(t)$ from its mean value.
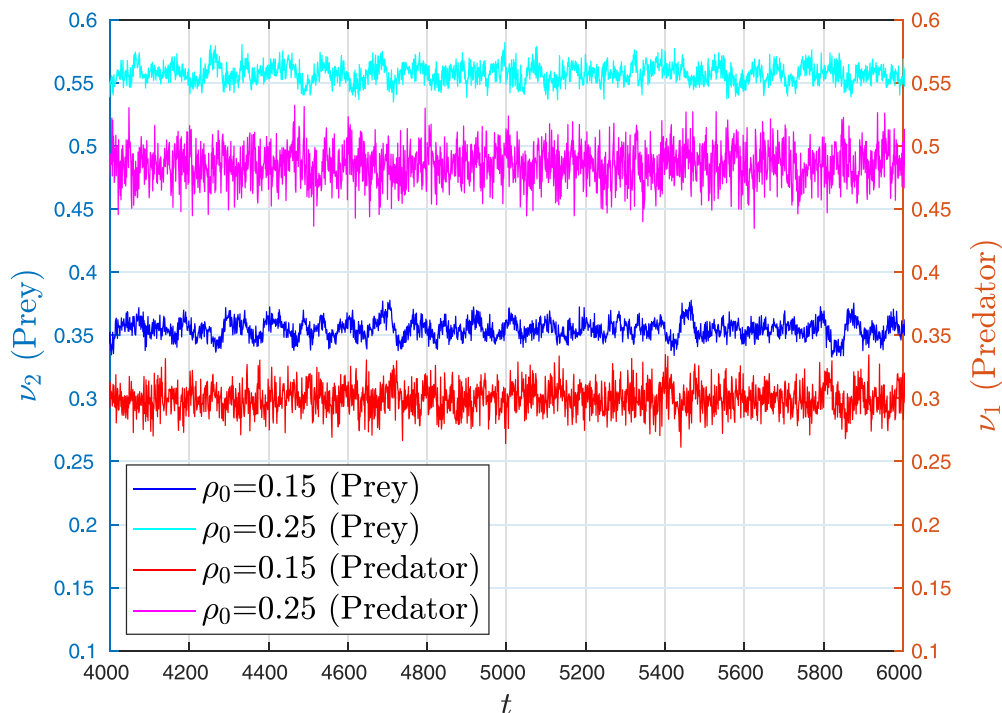
Figure 7. Collisional frequencies of predators (ν_1) and prey (ν_2) in the presence of obstacles (4-mers) at densities $\rho_0 = 0.15$, 0.25. Numerical results correspond to the set of probabilities $\mathcal{S}_1 = \{0.09, 0.05, 0.01, 0.15, 0.01\}$, and two densities $\rho_0 = 0.15$, 0.25 of 4-mers. Shown here are the temporal dependences of the ν_1 and ν_2 in the oscillatory region of the quasi-steady state, between $t_1 = 4000$ u.t. and $t_2 = 6000$ u.t..

Comparisons of the time-averaged WPS obtained for various obstacle lengths $k = 1, 2, 4, 8$ are shown in figure 9. We note that changing the length and shape of obstacles at a fixed density $\rho_0 = 0.15$ has almost no effect on the global WPS.

3.2.1. Coherence of the fluctuations In the absence of obstacles, the oscillations are persistently coherent, without the non-coherent breaks in the time-series $\tilde{N}_1(t)$ and $\tilde{N}_2(t)$ (see figures 5 and 6). In the following, we present the results of our analysis of the WCO between predators and prey obtained in the cases when the habitat is covered with obstacles at various concentrations $\rho_0 \leqslant 0.25$. We show that the presence of obstacles is responsible for the reversible shift from coherent to non-coherent oscillations.

In figure 10, we compare WCO for the two values of obstacle density, $\rho_0 = 0.15$, 0.25. For comparison, we show the results obtained for obstacles of very different lengths, namely, for monomers and 8-mers (table 1). The numerical results correspond to the set $\mathcal{S}_1 = \{0.09, 0.05, 0.01, 0.15, 0.01\}$ of probabilities that characterize the non-conservative processes. Thick solid lines indicate the 95% significance level. Arrows that indicate phase angles between fluctuations of the two species are only shown where the value of the WCO is greater than or equal to the threshold of 0.85. For lower density $\rho_0 = 0.15$, the dynamics can be characterized by regular oscillations in time with a nearly constant
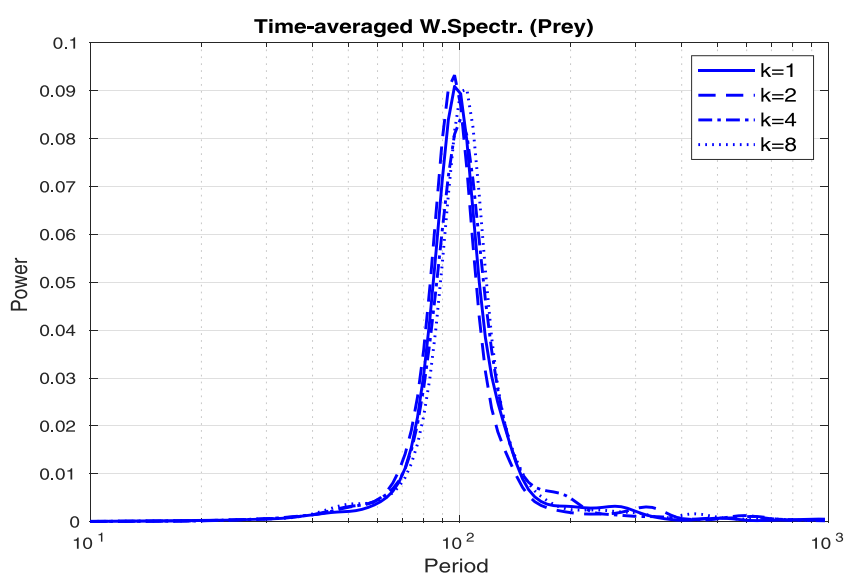
(a)

(b)
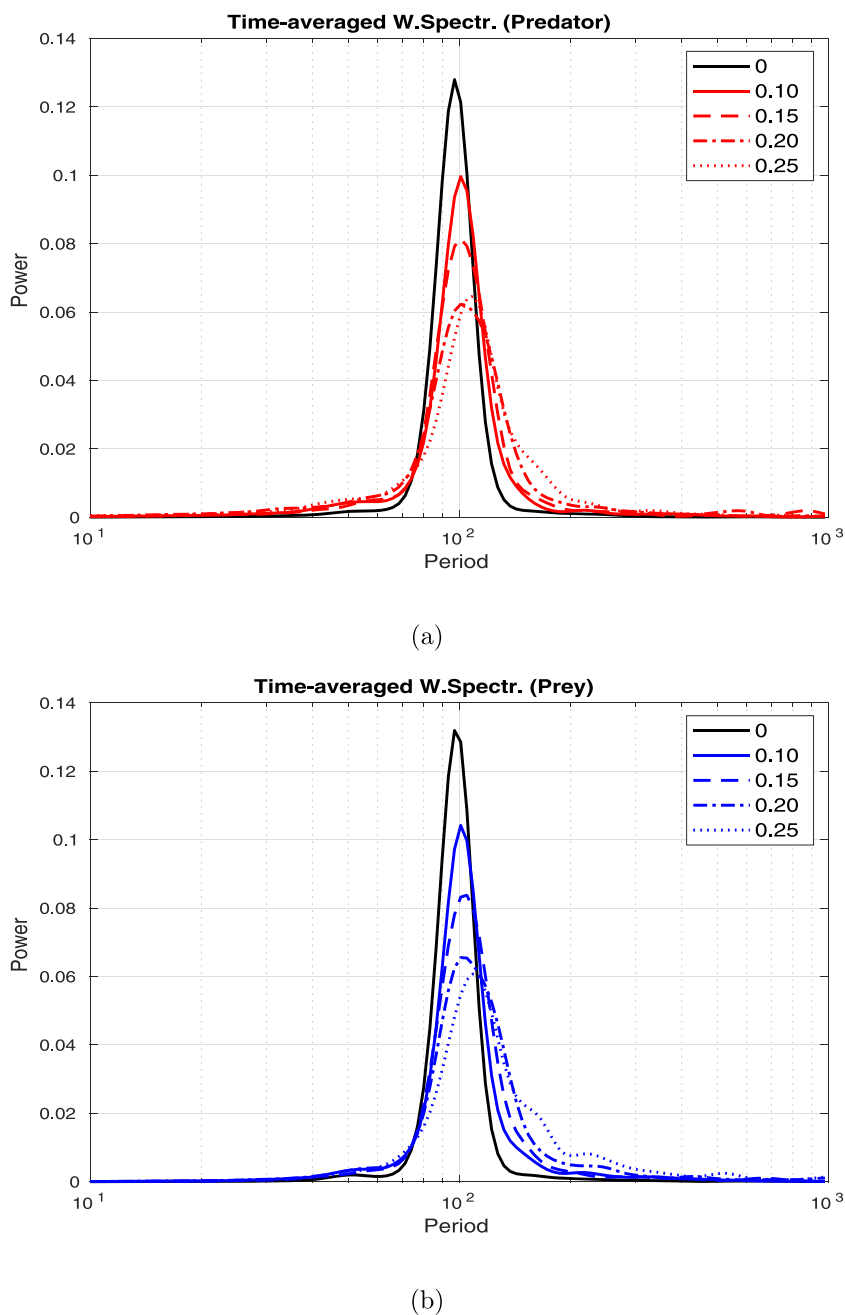
Figure 8. Time-averaged WPS of the predator and prey time-series, $\tilde{N}_1(t)$ (a) and $\tilde{N}_2(t)$ (b) respectively, obtained for 9-mers ($k = 9$) as obstacles at densities $\rho_0 = 0, 0.10, 0.15, 0.20, 0.25$. Probabilities that characterize the non-conservative processes are $\mathcal{S}_1 = \{0.09, 0.05, 0.01, 0.15, 0.01\}$.

predator–prey phase lag of about $\pi/2$ at frequencies corresponding to maximum WCO values (i.e. around $T_1 = 97$ u.t.). For higher density of obstacles $\rho_0 = 0.25$, significant regions of the time-frequency (period) plane reveals a wide distribution of different phase
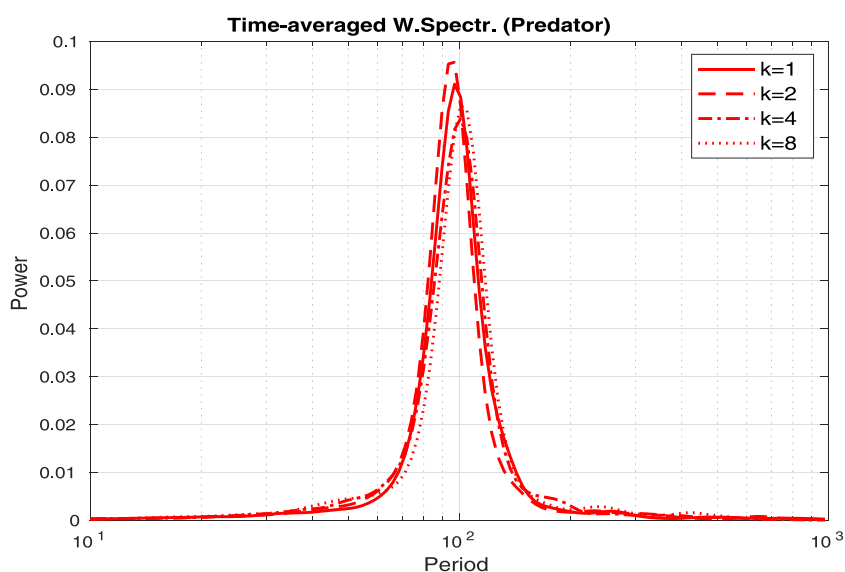
(a)

(b)

Figure 9. Time-averaged WPS of the predator and prey time-series, $\tilde{N}_1(t)$ (a) and $\tilde{N}_2(t)$ (b) respectively, obtained for various k-mers ($k = 1, 2, 4, 8$) as obstacles at density $\rho_0 = 0.15$. Probabilities that characterize the non-conservative processes are $\mathcal{S}_1 = \{0.09, 0.05, 0.01, 0.15, 0.01\}$.

angles. We also note a tendency for regions with significant WCO to be decomposed into disjoint areas, especially in the case of long obstacles (see figure 10(d)).

A representative example of the occurrence of short episodes of irregular, non-coherent oscillations without any significant phase relationship induced by the presence

(a) $k = 1$, $\rho_0 = 0.15$

(b) $k = 8$, $\rho_0 = 0.15$
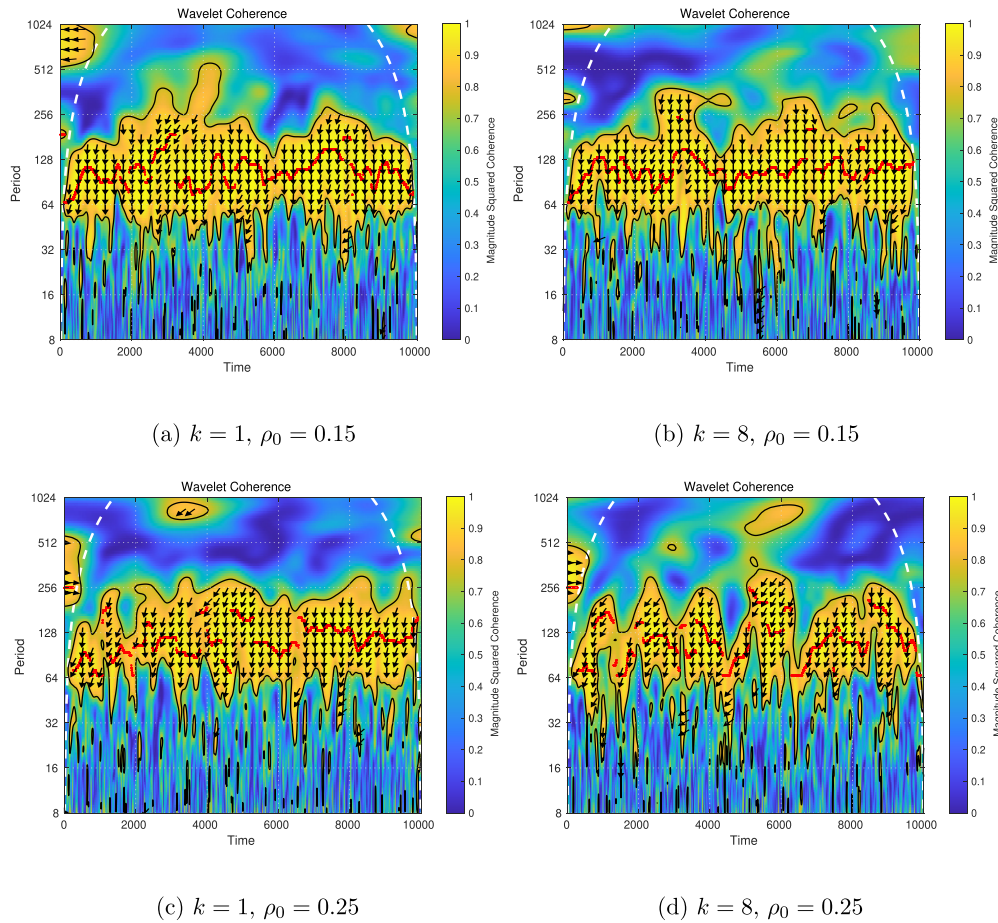
(c) $k = 1$, $\rho_0 = 0.25$

(d) $k = 8$, $\rho_0 = 0.25$
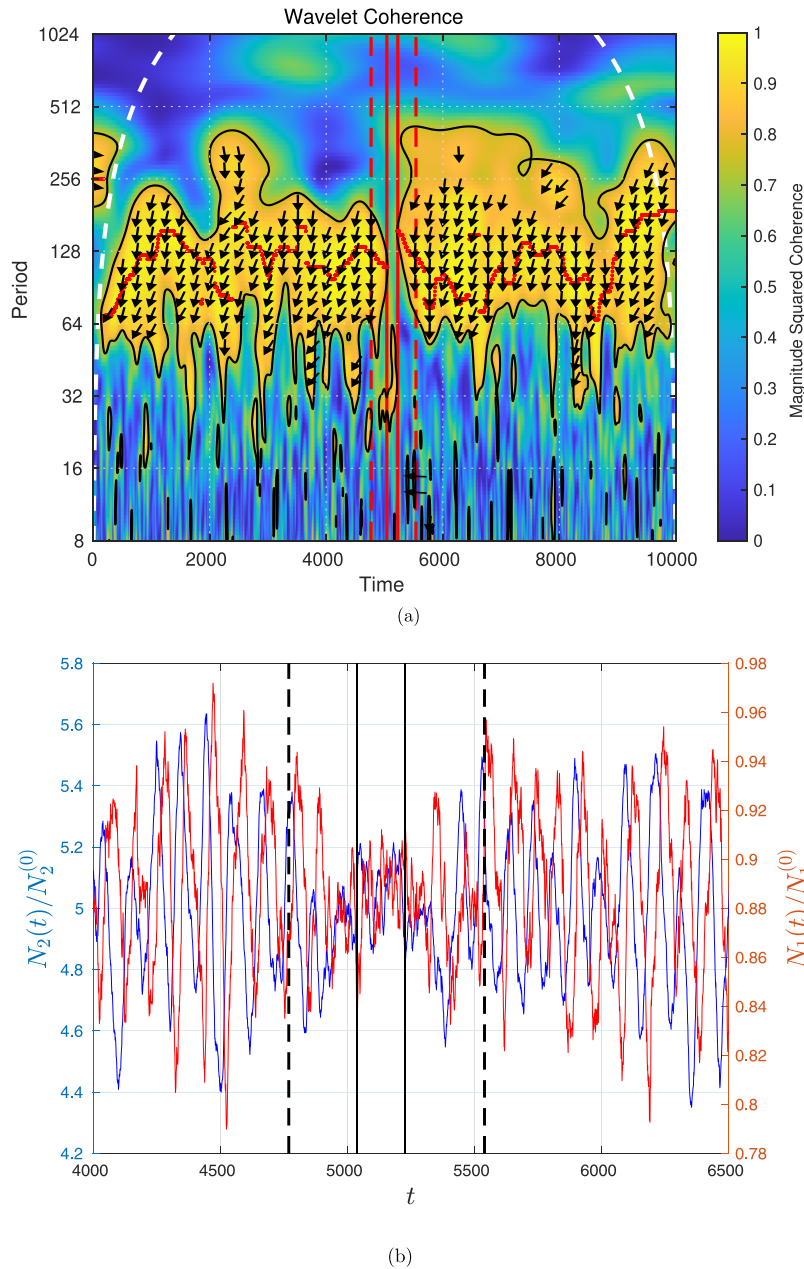
Figure 10. WCO between predators and prey, corresponding to time-series $\tilde{N}_1(t)$ and $\tilde{N}_2(t)$, obtained for monomers ($k = 1$) and 8-mers ($k = 8$) as obstacles, at two densities ρ_0: (a) $k = 1$, $\rho_0 = 0.15$; (b) $k = 8$, $\rho_0 = 0.15$; (c) $k = 1$, $\rho_0 = 0.25$; (d) $k = 8$, $\rho_0 = 0.25$. Values range from 0 (blue) to 1 (yellow). Cone of influence is indicated by the dashed white lines. Red dots indicate the instantaneous oscillation period $\tilde{s}(t)$ of the highest WCO within the prefixed period length band (64–256 u.t.). Significant areas (95% significance level) are enclosed by thin solid lines. Arrows indicate the phase angles between the fluctuations of the two species. We use the phase display threshold of 0.85, which shows phase arrows only where the coherence is greater than or equal to 0.85.

of obstacles is given in figure 11. The numerical results correspond to the set of probabilities $\mathcal{S}_1 = \{0.09, 0.05, 0.01, 0.15, 0.01\}$ and a high density $\rho_0 = 0.25$ of 9-mers as obstacles. Figure 11(a) shows the WCO between predators and prey obtained from the time-series shown in figure 11(b). In order to make it easier to connect the results on both panels, dashed vertical lines border an arbitrarily chosen time interval $t = 4770 - 5540$ u.t.

(a)

(b)

Figure 11. (a) WCO between predators and prey, corresponding to time-series $\tilde{N}_1(t)$ and $\tilde{N}_2(t)$, obtained for 9-mers ($k = 9$) as obstacles, at density $\rho_0 = 0.25$. Red dots indicate the instantaneous oscillation period $\tilde{s}(t)$ of the highest WCO within the prefixed period length band (64–256 u.t.). Significant areas (95% significance level) are enclosed by thin solid lines. Arrows indicate the phase angles between the fluctuations of the two species. We use the phase display threshold of 0.85, which shows phase arrows only where the coherence is greater than or equal to 0.85. (b) Shown here are the temporal dependencies of the normalized number of predators $\tilde{N}_1$ (red lines) and prey $\tilde{N}_2$ (blue lines) in the oscillatory region of the quasi-steady state, between $t_1 = 4000$ u.t. and $t_2 = 6500$ u.t. obtained under the same conditions as in panel (a). Dashed vertical lines on both panel border a time interval $t = 4770 - 5540$ u.t. Solid vertical lines at $t_1 = 5040$ u.t. and $t_2 = 5228$ u.t. indicate the time span of irregular oscillations.

Coherent oscillation regime is a contiguous time interval for which the dominant scale $\tilde{s}(t)$ is within a statistically significant area in the time-scale plane (see appendix). The time intervals that do not meet this condition constitute the non-coherent oscillation regimes. Solid vertical lines in figure 11 border a time interval without significant WCO between predator and prey. Non-coherent oscillations arise between $t_1 = 5040$ u.t. and $t_2 = 5228$ u.t. Indeed, the appearance of more irregular time-series can be observed in figure 11(b), in which the phase relationship between prey and predator is lost in oscillatory regions between solid vertical lines, although both populations continue to oscillate. Within significant regions of the time-frequency (period) plane, we observe that the predator density follows the prey density with a phase difference of $\Delta > \pi/2$. Dominant phase difference values $\tilde{\Delta}(t)$ (see appendix) range from $90°$ to $\approx 120°$, with a mean value of $\langle \tilde{\Delta} \rangle = 105° \pm 15°$ for the entire time interval. Since the dominant scale $\tilde{s}(t)$ constitutes the line of the strongest co-oscillating component of both signals in the time-scale plane, it can be concluded that value $\langle \tilde{\Delta} \rangle = 105° \pm 15°$ is the dominant predator—prey phase difference that characterizes coherent regions.

In the time range between dashed vertical lines in figure 11 ($\delta t = 4770 - 5540$ u.t.), we observe a reversible shift from coherent to non-coherent oscillations that are triggered by the presence of obstacles. Outside this region, oscillations with a dominant predator–prey phase difference $\langle \tilde{\Delta} \rangle \approx 105°$ are established. The central part inside this region corresponds to the regime of incoherent oscillations. However, inside significant areas that are enclosed between dashed vertical lines we detect predator–prey cycles with phase shift of $\pi/2$. Here, we observe that the regime of coherent oscillations gives way to a noncoherent time-series spontaneously, but the system also shows a tendency to return to the dominant dynamical regime with a defined phase relationship. It is important to note that the regime of incoherent oscillations also appears when another parameter set, $\mathcal{S}_2$, determines non-conservative processes. As in the case of parameter set $\mathcal{S}_1$, decoherence of oscillations occurs if the obstacle density is sufficiently high. This is confirmation that the presence of obstacles can induce incoherent oscillations, regardless of the characteristics of the non-conservative processes.

In figure 12, we show the scalograms and scale-averaged power spectra (SAWS) of the signals $\tilde{N}_1(t)$ and $\tilde{N}_2(t)$ obtained under the same conditions as in figure 11. Scale-averaged WPS is obtained by scale-averaging the magnitude-squared scalogram over all scales. In fact, the SAWS is a time-series of the average variance in a certain band [47]. In the case of figure 11, it is the 16–1024 u.t. band on the period scale. Thus, SAWS can be used to examine modulation of one time-series by another, or modulation of one frequency by another within the same time-series. The variance plot for predators and prey (2nd and 4th panel in figure 12) shows a distinct period between vertical lines when variance is low. Both time series show consistent changes over time. According to figures 11 and 12, we can see that periods with low values of SAWS coincide with regions without significant WCO between predator and prey.

(a)

(b)
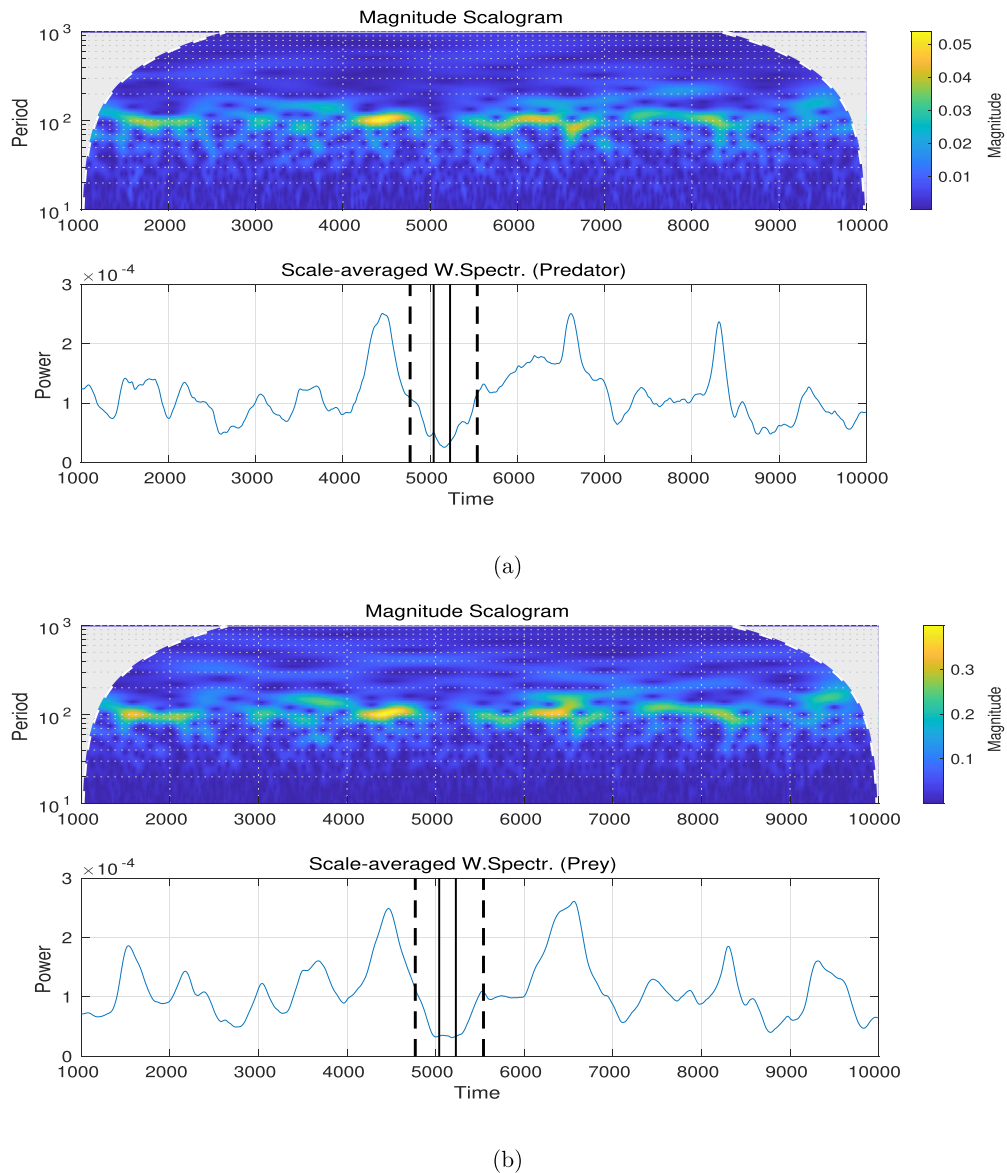
Figure 12. Scalograms and SAWS of the predator and prey time-series, $\tilde{N}_1(t)$ (a) and $\tilde{N}_2(t)$ (b) respectively, obtained for 9-mers ($k=9$) as obstacles at density $\rho_0 = 0.25$. Data correspond to the quasi-steady state regime of evolution ($t > 1000$ u.t.). SAWS is obtained by scale-averaging the magnitude-squared scalogram over all scales. As in figure 11, dashed vertical lines on both panels border a time interval $t = 4770 - 5540$ u.t.. Solid vertical lines at $t_1 = 5040$ u.t. and $t_2 = 5228$ u.t. indicate time span of irregular oscillations.

4. Concluding remarks

In this paper, we have developed an intuitively plausible model for understanding the impact of habitat spatial heterogeneities on the population dynamics of predator–prey

systems. We study a stochastic lattice model describing group chase and escape with sight-limited predators and prey using numerical simulations. Five probabilities that control the breeding and physiological dying of predators and prey were introduced into the model. The habitat heterogeneities are built by randomly selecting a fraction of the sites of the square lattice that are considered forbidden for the species.

In the absence of obstacles, numerical simulations reveal sustained oscillations with a nearly constant predator–prey phase difference. Numerical simulations have shown that changing the probabilities for non-conservative processes can increase or decrease the period of coherent oscillations in the abundance of species and change the relative lag between coherent components. After introducing obstacles into the model, we observe the breaks in the oscillation regimes, with random transitions between coherent and non-coherent oscillating regimes. Our model suggests that stochasticity introduced by obstacles is probably responsible for the reversible shift from coherent to non-coherent oscillations. At a sufficiently small scale, heterogeneities in the environment can decrease the ability of predators to catch prey by modifying the movement of individuals. Indeed, obstacles reduce the spatial spread of particles. By changing the trajectory of predators, obstacles increase the probability that a predator explores a place he had already gone through and previously cleared of prey. Therefore, obstacles decrease the encounter rate of the predator with prey. Furthermore, predators could lose time to handle obstacles they encounter during their search for prey. Accumulation of a high number of obstacles encountered could decrease the time available to search for prey. Consequently, the handling of obstacles could also decrease the attack rate. We consider that obstacles, at sufficiently high densities, decompose the habitat into areas of various sizes and shapes, where predators and prey are partially isolated from the rest of the habitat. The local dynamics in these areas are determined by the size and shape of these regions, due to the influence of obstacles on, for example, encounter and attack rates. Impaired communication among individuals in different habitat areas further promotes the development of different dynamics within these isolated units. In other words, the spatial separation of habitats leads to the development of local oscillatory regimes with different phase relationships. Consequently, density fluctuations of obstacles make predator–prey dynamics in different parts of the habitat very heterogeneous. This heterogeneity of the coexistence dynamics reduces or even prevents the establishment of overall oscillations with a defined phase relationship. Note that we have shown that periods with low values of SAWS coincide with short episodes of irregular, non-coherent oscillations (figure 12). If the signal of interest is contaminated by noise or interference, it can affect the wavelet analysis and result in small scale-averaged power values. Noisy signals often have components that may not contribute significantly to the overall power at each scale, leading to smaller values in the scale-averaged spectra. In general, stochasticity or external perturbations can obscure or prevent predator–prey oscillations, and our simulations suggest that stochasticity introduced by obstacles is probably responsible for the reversible shifts from coherent to more-erratic oscillations that we observe in our model.

Here, obstacles are represented by non-overlapping k-mers that are randomly placed on the lattice. It would be interesting to perform a similar investigation with obstacles of various shapes. We can introduce anisotropy in the deposition procedure for obstacle

shapes. This simple modification introduces a preferential direction in the obstacle orientations and, depending on the aspect ratio of the deposited shapes, imposes specific 'patterning' on the habitat. This would allow us to study the role that the spatial structure of the habitat plays in the pursuit–evasion processes.

Acknowledgments

Appendix. Wavelet analysis

The wavelet transform decomposes signals over dilated and translated functions called 'mother wavelets' $\psi(\tau)$. Throughout our analysis, we used the Morlet wavelet $\psi(\tau) = \pi^{-1/4}\exp(i\omega_0\tau)\exp(-\tau^2/2)$. The CWT of a signal $x(t)$ is calculated as the convolution of the signal with a localized complex-valued wavelet function $\psi(\tau)$ centered at time t and dilated by the scale parameter s:

$$W_x(s,t) = \frac{1}{s^{1/2}} \int \mathrm{d}t' x(t')\psi^*\left(\frac{t'-t}{s}\right). \tag{A1}$$

Here, the asterisk denotes the complex conjugate. The wavelet coefficients, $W_x(s,t)$, represent the contribution of the scales (the s values) to the signal at different time positions (the t values).

To quantify the statistical relationship between two non-stationary signals $x(t)$ and $y(t)$, the WCS is defined as the smoothed product of the corresponding wavelet transforms:

$$W_{x,y}(s,t) = \langle W_x(s,t)W_y^*(s,t)\rangle. \tag{A2}$$

Here, $\langle\cdots\rangle$ denotes a smoothing operator in both scale and time. The WCS is a measure of the distribution of power of two signals. Local WPS of a signal $x(t)$ at time t and scale s is defined as $W_{x,x}(s,t) = \langle W_x(s,t)W_x^*(s,t)\rangle$. The global (time-averaged) WPS is defined as the time average of the local WPS and measures the averaged variance of the signal $x(t)$ at scale s. We use the maximum of global WPS to estimate the mean oscillation period of the signal.

WCO is defined as the amplitude of the WCS divided by the square roots of the two local WPS:

$$\mathrm{WCO}_{x,y}(s,t) = \frac{|W_{x,y}(s,t)|}{\sqrt{W_{x,x}(s,t)}\sqrt{W_{y,y}(s,t)}}. \tag{A3}$$

The WCO estimates the relationship between the two signals at time t and scale s, normalized into the range $0 \leqslant \mathrm{WCO} \leqslant 1$.

The dominant scale $\tilde{s}(t)$ is defined for every time instance t as the scale parameter that has maximum WCO at time t over all scales in a prefixed band $[s_1, s_2]$. The statistical significance of the WCO is tested against red noise using Monte Carlo (MC) methods [52, 53]. Surrogate time series ($N = 1000$) are generated with the same first-order autoregression coefficients as the original time series. For each pair, the WCO is calculated and then the significance level is estimated for each scale from the ensemble of MC results, using a 95% significance level. As a coherent oscillation regime, we define a maximum contiguous time interval for which the dominant scale $\tilde{s}(t)$ is inside a statistically significant area (95% significance level) in the time-scale plane. Inserting dominant scale $\tilde{s}(t)$ into the WCS yields the dominant phase difference $\tilde{\Delta}(t)$ between the two signals at every time instance.

References

[1] Lotka A J 1926 *Elements of Physical Biology* (*Science Progress in the Twentieth Century (1919–1933)*) vol 21 (Springer) p 341

[2] Volterra V 1928 Variations and fluctuations of the number of individuals in animal species living together *ICES J. Mar. Sci.* **3** 3

[3] Rosenzweig M L and MacArthur R H 1963 Graphical representation and stability conditions of predator-prey interactions *Am. Nat.* **97** 209

[4] Bulmer M 1976 The theory of prey-predator oscillations *Theor. Popul. Biol.* **9** 137

[5] Elton C and Nicholson M 1942 The ten-year cycle in numbers of the lynx in Canada *J. Anim. Ecol.* **11** 215

[6] Utida S 1957 Cyclic fluctuations of population density intrinsic to the host-parasite system *Ecology* **38** 442

[7] Luckinbill L S 1974 The effects of space and enrichment on a predator-prey system *Ecology* **55** 1142

[8] Gilg O, Hanski I and Sittler B 2003 Cyclic dynamics in a simple vertebrate predator-prey community *Science* **302** 866

[9] Sengupta A, Kruppa T and Löwen H 2011 Chemotactic predator-prey dynamics *Phys. Rev.* E **83** 031914

[10] Weng T, Yang H, Gu C, Zhang J, Hui P and Small M 2019 Predator-prey games on complex networks *Commun. Nonlinear Sci. Numer. Simul.* **79** 104911

[11] Baggio J A, Salau K, Janssen M A, Schoon M L and Bodin Orjan 2010 Landscape connectivity and predator–prey population dynamics *Landsc. Ecol.* (Springer) **26** 33

[12] Stucchi L, Galeano J and Vasquez D A 2019 Pattern formation induced by intraspecific interactions in a predator-prey system *Phys. Rev.* E **100** 062414

[13] Chakraborty D, Bhunia S and De R 2020 Survival chances of a prey swarm: how the cooperative interaction range affects the outcome *Sci. Rep.* **10** 8362

[14] Patwardhan S, De R and Panigrahi P K 2020 Survival probability of a lazy prey on lattices and complex networks *Eur. Phys. J.* E **43** 53

[15] Samhouri J F, Stier A C, Hennessey S M, Novak M, Halpern B S and Levin P S 2017 Rapid and direct recoveries of predators and prey through synchronized ecosystem management *Nat. Ecol. Evol.* **1** 0068

[16] Keim J L, DeWitt P D, Wilson S F, Fitzpatrick J J, Jenni N S and Lele S R 2021 Managing animal movement conserves predator–prey dynamics *Front. Ecol. Evol.* **19** 379

[17] Guiden P W, Bartel S L, Byer N W, Shipley A A and Orrock J L 2019 Predator–prey interactions in the anthropocene: Reconciling multiple aspects of novelty *Trends Ecol. Evol.* **34** 616

[18] Brown J S 1988 Patch use as an indicator of habitat preference, predation risk and competition *Behav. Ecol. Sociobiol.* **22** 37

[19] Holt R D 1984 Spatial heterogeneity, indirect interactions and the coexistence of prey species *Am. Nat.* **124** 377

[20] Serrouya R, Seip D R, Hervieux D, McLellan B N, McNay R S, Steenweg R, Heard D C, Hebblewhite M, Gillingham M and Boutin S 2019 Saving endangered species using adaptive management *Proc. Natl Acad. Sci.* **116** 6181

[21] Šćepanović J R, Karač A, Jakšić Z M, Budinski-Petković L and Vrhovac S B 2019 Group chase and escape in the presence of obstacles *Physica* A **525** 450

[22] Šćepanović J, Jakšić Z, Budinski-Petković L and Vrhovac S 2021 Long-term effects of abrupt environmental perturbations in model of group chase and escape with the presence of non-conservative processes *Physica A* **580** 126156
[23] Kamimura A and Ohira T 2010 Group chase and escape *New J. Phys.* **12** 053013
[24] Kamimura A and Ohira T 2019 *Group Chase and Escape: Fusion of Pursuits-Escapes and Collective Motions* (Springer)
[25] Janosov M, Virágh C, Vásárhelyi G and Vicsek T 2017 Group chasing tactics: how to catch a faster prey *New J. Phys.* **19** 053003
[26] Nishi R, Kamimura A, Nishinari K and Ohira T 2012 Group chase and escape with conversion from targets to chasers *Physica A* **391** 337
[27] Sato M 2012 Chasing and escaping by three groups of species *Phys. Rev.* E **85** 066102
[28] Iwama T and Sato M 2012 Group chase and escape with some fast chasers *Phys. Rev.* E **86** 067102
[29] Saito T, Nakamura T and Ohira T 2016 Group chase and escape model with chasers' interaction *Physica A* **447** 172
[30] Angelani L 2012 Collective predation and escape strategies *Phys. Rev. Lett.* **109** 118104
[31] Yang S, Jiang S, Jiang L, Li G and Han Z 2014 Aggregation increases prey survival time in group chase and escape *New J. Phys.* **16** 083006
[32] Rozenfeld A F and Albano E V 2001 Critical and oscillatory behavior of a system of smart preys and predators *Phys. Rev.* E **63** 061907
[33] Wang H, Han W and Yang J 2017 Group chase and escape with sight-limited chasers *Physica A* **465** 34
[34] Travis J 2007 Do wandering albatrosses care about math? *Science* **318** 742
[35] Pekalski A 2004 A short guide to predator-prey lattice models *Comput. Sci. Eng.* **6** 62
[36] Rozenfeld A and Albano E 1999 Study of a lattice-gas model for a prey–predator system *Physica A* **266** 322
[37] Boccara N, Roblin O and Roger M 1994 Automata network predator-prey model with pursuit and evasion *Phys. Rev.* E **50** 4531
[38] Droz M and Pękalski A 2001 Coexistence in a predator-prey system *Phys. Rev.* E **63** 051909
[39] Fussmann G F, Ellner S P, Shertzer K W and Hairston N G Jr 2000 Crossing the hopf bifurcation in a live predator-prey system *Science* **290** 1358
[40] Benincà E, Jöhnk K D, Heerkloss R and Huisman J 2009 Coupled predator–prey oscillations in a chaotic food web *Ecol. Lett.* **12** 1367
[41] Evans J W 1993 Random and cooperative sequential adsorption *Rev. Mod. Phys.* **65** 1281
[42] Budinski-Petković L, Lončarević I, Dujak D, Karač A, Šćepanović J R, Jakšić Z M and Vrhovac S B 2017 Particle morphology effects in random sequential adsorption *Phys. Rev.* E **95** 022114
[43] Luckinbill L S 1973 Coexistence in laboratory populations of paramecium aurelia and its predator didinium nasutum *Ecology* **54** 1320
[44] Hauzy C, Tully T, Spataro T, Paul G and Arditi R 2010 Spatial heterogeneity and functional response: an experiment in microcosms with varying obstacle densities *Oecologia* **163** 625
[45] Blasius B, Rudolf L, Weithoff G, Gaedke U and Fussmann G F 2020 Long-term cyclic persistence in an experimental predator–prey system *Nature* **577** 226
[46] Tarasevich Y Y, Laptev V V, Vygornitskii N V and Lebovka N I 2015 Impact of defects on percolation in random sequential adsorption of linear *k*-mers on square lattices *Phys. Rev.* E **91** 012109
[47] Torrence C and Compo G P 1998 A practical guide to wavelet analysis *Bull. Am. Meteorol. Soc.* **79** 61
[48] Cazelles B, Chavez M, Berteaux D, Ménard F, Vik J O, Jenouvrier S and Stenseth N C 2008 Wavelet analysis of ecological time series *Oecologia* **156** 287
[49] Begon M, Townsend C R and Harper J L 2006 *Ecology: From Individuals to Ecosystems* 4th edn (Blackwell Publishing)
[50] Vandewalle N, Galam S and Kramer M 2000 A new universality for random sequential deposition of needles *Eur. Phys. J.* B **14** 407
[51] Cornette V, Ramirez-Pastor A J and Nieto F 2003 Percolation of polyatomic species on a square lattice *Eur. Phys. J.* B **36** 391
[52] Grinsted A, Moore J C and Jevrejeva S 2004 Application of the cross wavelet transform and wavelet coherence to geophysical time series *Nonlinear Process. Geophys.* **11** 561
[53] Si B C 2008 Spatial scaling analyses of soil physical properties: a review of spectral and wavelet methods *Vadose Zone J.* **7** 547